Available online at www.sciencedirect.com
SCIENCE DIRECT®
Computers in Industry 56 (2005) 442–456
COMPUTERS IN INDUSTRY
www.elsevier.com/locate/compind

CAD/CAE/CAM integration for increasing the accuracy of mask rapid prototyping system

You-Min Huang *, Hsiang-Yao Lan

Department of Mechanical Engineering, National Taiwan University of Science and Technology, 43 Keelung Road, Section 4, Taipei 106, Taiwan

Received 5 July 2004; accepted 13 January 2005
Available online 17 March 2005

Abstracts

Stereolithography is a rapid prototyping (RP) process that uses photopolymers as the raw materials from which the prototypes are built. The photo-polymeric RP system uses lasers or other light sources to expose selectively the surface of the liquid resin. The absorption of energy causes photo-polymerization that changes the liquid resin into a solid, expanding the cured volume expanding but shrinking simultaneously. The volume shrinkage and curl distortion of the resin during photo-polymerization are the main reasons for the poor accuracy of the built prototype, especially when the part is hollow, in which case the bending is greater because of the bending stress and cannot be compensated for. Normally, a designer builds a support in this stage to limit the further bending and deformation of the prototype. However, after the support has been removed from the built prototype, the geometric profile is easily damaged and deformed, so time is wasted. This study initially uses dynamic finite element simulation code to simulate photo-polymerization, to determine the distortion of the outer profile of the part and thus reduce the deformation. Then, a reverse distortion correction is applied to the outer profile of the part. A new reverse compensation CAD model is produced and loaded into a RP machine for practical prototype processing, to increase the accuracy of the process. Finally, the ''H-4'' diagnostic part is used as an example to verify the experimental results. The results of the simulation and experiment on the final after compensation were accurate.

Keywords: Computer-aided engineering; Stereolithography; Rapid prototyping; Finite element method; Curl distortion

1. Introduction

Industrial competition has accelerated the development of rapid prototyping (RP) systems. The use of rapid prototyping systems can accelerate R&D and the market-placement of products. Consequently, reducing the processing time and ensuring the precision of the production have dominated the improvement of rapid prototyping systems.

In a rapid prototyping system, the optical light source used in the light source transmission structure can be a point light source (such as a laser or LED light), a linear light source (such as an LED-array), or

* Corresponding author. Tel.: +886 2 2737 6487; fax: +886 2 2737 6460.
E-mail addresses: ymhuang@mail.ntust.edu.tw (Y.-M. Huang), lanhf.hy@msa.hinet.net (H.-Y. Lan).

0166-3615/$ – see front matter © 2005 Elsevier B.V. All rights reserved.
doi:10.1016/j.compind.2005.01.002

a source of light uniformly distributed over an area. Each of which is produced to meet the requirements of the designer. The light source used herein is an area source of Digital Light Processor (DLP) light. The solidification of a region exposed to this rapid prototyping is based on the principles of the exposure and sheltering of a mask, so the optical light source passes through the exposed portion onto the polymerized resin that thus undergoes polymerization. Therefore, the heating is uniform, the dimensions of the product are stable, and the rate of production is fast, which factors all effectively reduce the processing time of the products. It is therefore one of the most popular rapid prototyping systems.

The poor accuracy of the constructed prototype is caused mainly by the volume shrinkage of the resin during photo-polymerization. The use of the light source produces free radicals that promote photo-polymerization, and the bonding of small molecules (monomers) into large molecules (polymers) that comprise several monomer units [1]. Linking is exothermic and curing in a tiny volume instantly increases the temperature. The cured volume expands as the exothermic reaction proceeds, and shrinks after the temperature is lowered after the liquid photopolymer, which is not cured, reaches thermal equilibrium.

Shrinkage is the most serious cause of errors in the build-up process. Hence, much research has focused on observing and simulating the problem of shrinkage. Narahara et al. [2] set up experimental apparatus to elucidate the basic dynamic solidification during photo-polymerization. Bugeda et al. [3] developed a finite element program to simulate the structural behavior of SL resins using a linear elastic model with a constant Young's modulus and a constant Poisson ratio. Tanaka et al. [4] developed a model of dynamic resin materials based on the properties of the resin after photo-polymerization.

The solid ground curing (SGC) system [1], commercialized by Cubital Company, is a typical mask-type stereolithography RP system. Huang et al. [5] developed an innovative RP system, using a liquid crystal display (LCD), to generate a dynamic mask for direct mask photo curing (DMPC). Murakami et al. [6] used refrigerated stereolithography to form mask patterns by drawing a special sol–gel transformable photopolymer resin. Micro RP systems represent another area of become recent development. The

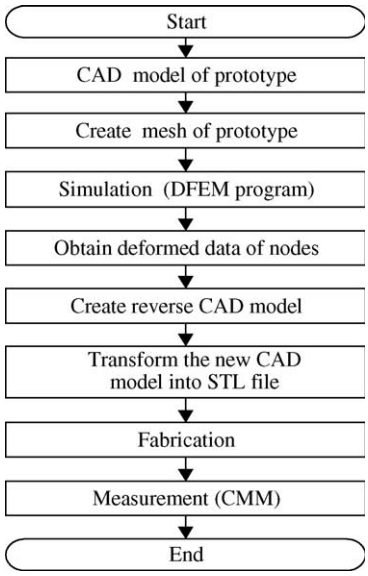

Fig. 1. The flowchart of the reverse compensation process.

mask-based stereolithographic technique and optical components have been used to yield the required resolution. For example, Hatashi et al. [7] used a thin film transistor LCD to create a mask pattern and without lamination, to fabricate optical lenses. Huang

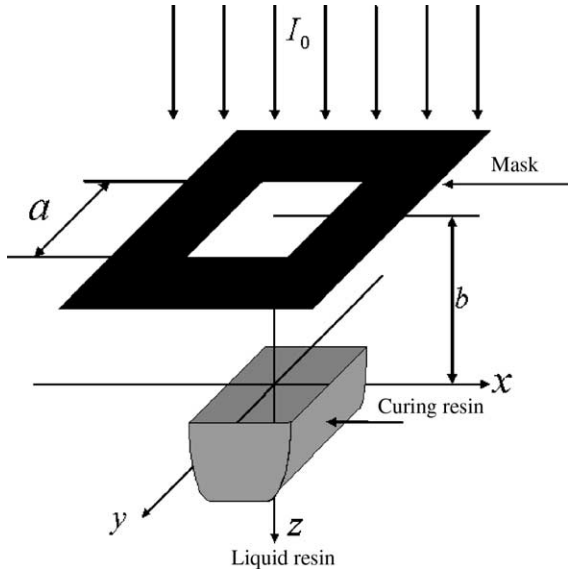

Fig. 2. Schematic of energy distribution of square mask type prototyping.

and Jiang [8,9] used the dynamic finite element method (DFEM) to simulate stereolithography, based on the dynamic properties of photo-polymerization. Many of these studies have focused on analyzing the effect of curing during build-up. However, only a few studies have sought to improve curl distortion, especially when the built part is hollow; this bending is very obvious and cannot be compensated by bending stress.

This study presents verification and validation methods to improve the curl distortion using low-cost equipment. First, The equation based on DFEM theory [8,9], is used herein in numerical simulation with input parameters that correspond to a practical processes. Then, the distortion of the built parts is predicted. Second, reverse distortion compensation is used to produce a new CAD model that is based on the predicted distortion. Thirdly, the new CAD model is converted into a stereolithographic (STL) file. Finally, this new STL file is sent to a RP machine for further processing. Accordingly, the low-cost machines greatly improve the accuracy of the part. The final results of the simulation and experiment are compared. Fig. 1 shows a flowchart of this process.

2. Numerical analysis

A modified mathematical model is proposed, based on the aforementioned reference and experimental

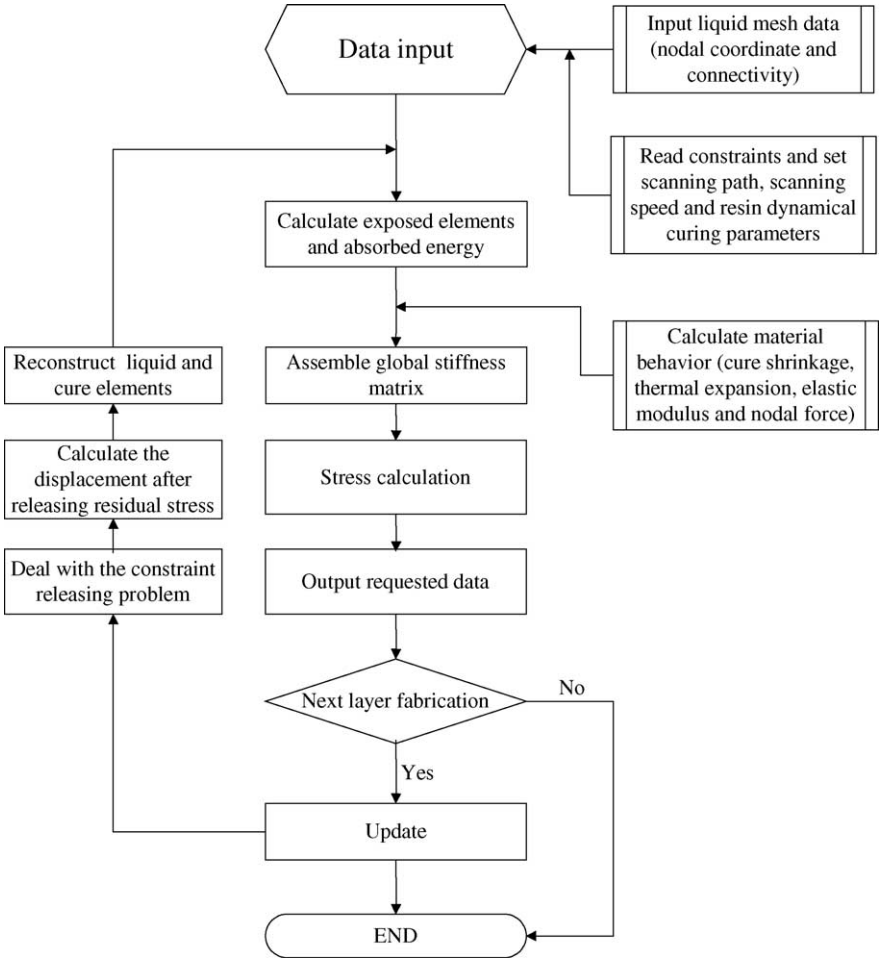

Fig. 3. The flowchart of the simulation process.

observations of the curing process for mask-type stereolithographic systems. This process is a phase transition from the liquid state to the solid state, proving that all factors are functions of the duration of the exposure to light, and the intensity of that light.

2.1. Dynamic finite element method

Huang and Jiang proposed a dynamic solidification model of photo-polymerization [8,9]. The behavior of the cure resin is a function of the intensity of that light I and the elapsed time t. The uncured liquid becomes more viscous as it absorbs the heat produced by the cured resin. For the convenience to express, in this paper substitutes the strain rate $\{\dot{\varepsilon}\}$ for the increment of strain $\{\Delta\varepsilon\}$. Therefore, the deformation of resin consists of the following elements. [10]

$$\{\dot{\varepsilon}\} = \{\dot{\varepsilon}^{\mathrm{e}}\} + \{\dot{\varepsilon}^{\mathrm{T}}\} + \{\dot{\varepsilon}^{\mathrm{v}}\} + \{\dot{\varepsilon}^{\gamma}\} + \{\dot{\varepsilon}^{\mathrm{p}}\} \tag{1}$$

where $\{\dot{\varepsilon}^{\mathrm{e}}\}$ represents the elastic strain rate; $\{\dot{\varepsilon}^{\mathrm{v}}\}$ is the viscous strain rate that is the function of time, so it can be expressed as $\{\sigma(t)\}$ [11]; $\sigma(t)$ is the viscous stress that is the function of time (t); $\{\dot{\varepsilon}^{\mathrm{T}}\}$ is the thermal strain rate that can be rewritten as $\{\alpha\dot{T}\}$; $\{\dot{\varepsilon}^{\gamma}\}$ is the strain rate caused by cure shrinkage and is given by $\Delta\beta(I, t)$; and $\{\dot{\varepsilon}^{\mathrm{p}}\}$ is the plastic strain rate. During photo-polymerization, the plastic strain is low and can be neglected. In the case in which $\{\dot{\sigma}\}$ equals $[D^{\mathrm{e}}]\{\dot{\varepsilon}\}$ and $\{\dot{\varepsilon}\}$ equals $[B]\{\dot{u}\}$, substituting the above relationship and $\int_v [B]^{\mathrm{T}}\,\mathrm{d}V$ into Eq. (1), yields the following equation:

$$\int_v [[B]^{\mathrm{T}}[D^{\mathrm{e}}][B]\{\dot{u}\} - [B]^{\mathrm{T}}\{\sigma\} - [B]^{\mathrm{T}}(3k)\{\alpha\dot{T} + \Delta\beta(I)\}]\,\mathrm{d}V = 0 \tag{2}$$

Consequently, the constitutive equation in the dynamic finite element analysis of the stereolithographic process can be expressed as

$$[K]\{\dot{u}\} - \{\dot{f}\} = 0 \tag{3}$$

where

$$[K] = \int_v [[B]^{\mathrm{T}}[D^{\mathrm{e}}][B]]\,\mathrm{d}V \tag{4}$$

$$\{\dot{f}\} = \int_v [[B]^{\mathrm{T}}\{\sigma\} + [B]^{\mathrm{T}}(3k)\{\alpha\dot{T} + \Delta\beta(I)\}]\,\mathrm{d}V \tag{5}$$

In the above equation, $[K]$ is the stiffness matrix; $\{\dot{u}\}$ is the increment in nodal displacement; $\{\dot{f}\}$ is increment in the effective nodal force; $[B]$ represents the strain rate–velocity matrix; $[B]^{\mathrm{T}}$ is the transpose of the matrix $[B]$; $\lfloor D^{\mathrm{e}} \rfloor$ is the stress–strain matrix; V is the volume of the reaction area; $\{\sigma\}$ represents the nodal viscous stress that is the function of time (t); k is the volume modulus; α is the linear expansion coefficient; $\dot{T}$ is the increment in temperature, and $\Delta\beta(I)$ is defined

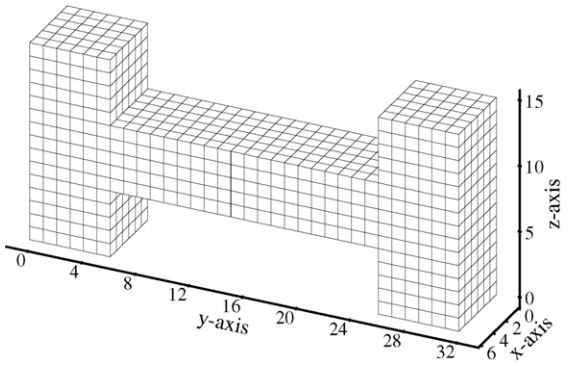

Fig. 4. FEM liquid mesh of "H-4" diagnostic part (units: mm).

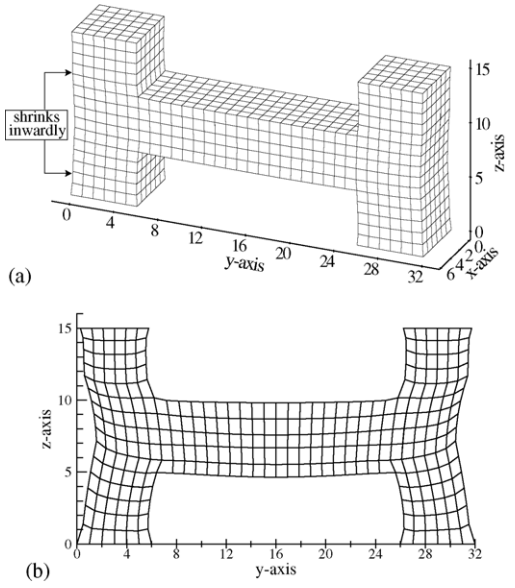

Fig. 5. The deformation of "H-4" part in simulation (units: mm). (a) Three-dimension deformation. (b) Two-dimension deformation (for convenience of observation, the distortion of every node is magnified five times).

as the strain associated with cure shrinkage, which is a function of the intensity of that light (I) and elapsed time (t).

2.2. Energy distribution in mask type prototyping

As light passes through the mask onto the surface of the resin, the distribution and uniformity of the diffusion of the energy on the surface affects the thickness of solidified layers. Therefore, the energy of the light that passes through the mask and is projected onto the surface of the resin must be calculated using a mathematical model to determine the energy of the mask. A square of side a is considered as an example. The energy intensity of the light source is I_0. The central point of the square mask is defined as $x = 0$ and $y = 0$, with an energy as depicted schematically in Fig. 2. After the light had passed through the mask, the intensity at any point in the square profile is given by [12]

$$I_d = \tfrac{1}{4} I_0 (C_x^2 C_y^2 + C_x^2 S_y^2 + S_x^2 C_y^2 + S_x^2 S_y^2) \tag{6}$$

where the relative coefficients, C and S, are defined as follows:

$$C_x = \int_{p_1}^{p_2} \cos(0.5\pi u^2)\,\mathrm{d}u \tag{7}$$

$$S_x = \int_{p_1}^{p_2} \sin(0.5\pi u^2)\,\mathrm{d}u \tag{8}$$

$$C_y = \int_{q_1}^{q_2} \cos(0.5\pi u^2)\,\mathrm{d}u \tag{9}$$

$$S_y = \int_{q_1}^{q_2} \sin(0.5\pi u^2)\,\mathrm{d}u \tag{10}$$

where

$$p_1 = \frac{2}{\sqrt{m}}\left(\frac{x}{a} - 0.5\right) \tag{11}$$

$$p_2 = \frac{2}{\sqrt{m}}\left(\frac{x}{a} + 0.5\right) \tag{12}$$

$$q_1 = \frac{2}{\sqrt{m}}\left(\frac{y}{a} - 0.5\right) \tag{13}$$

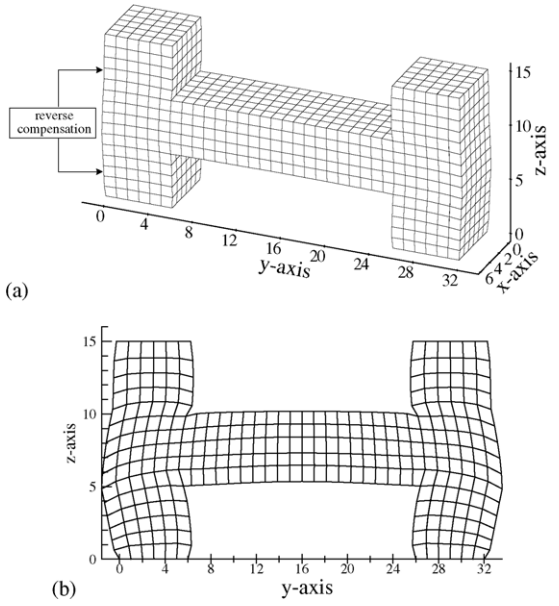

Fig. 6. The reverse compensation CAD mesh of "H-4" part in simulation (units: mm). (a) Three-dimension deformation. (b) Two-dimension deformation (for convenience of observation, the distortion of every node is magnified five times).

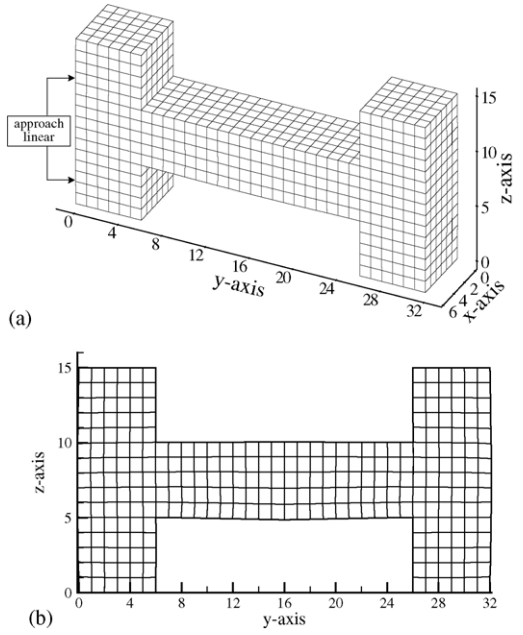

Fig. 7. The after compensation CAD mesh of "H-4" part in simulation (units: mm). (a) Three-dimension deformation. (b) Two-dimension deformation (for convenience of observation, the distortion of every node is magnified five times).

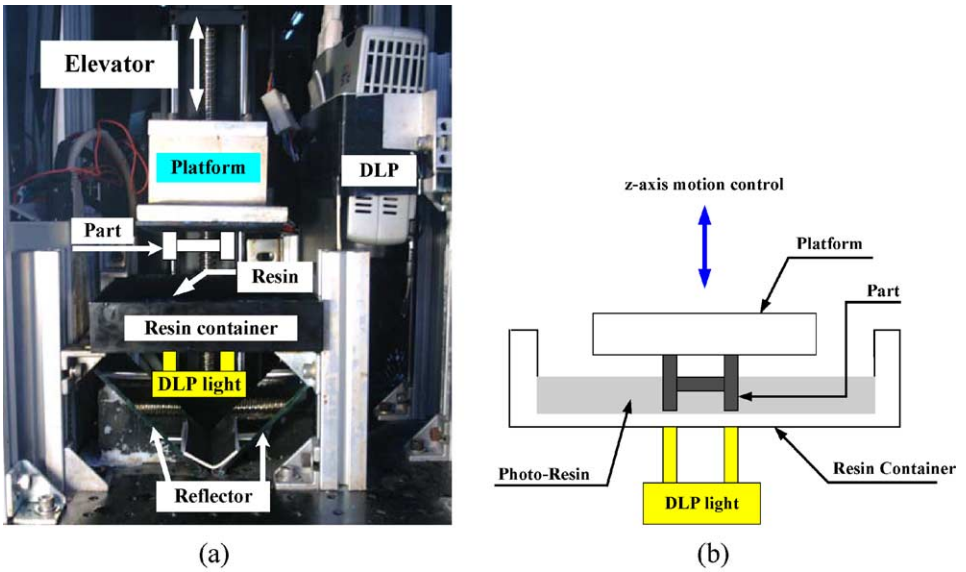

Fig. 8. Mask-type RP system by using DLP technique. (a) Integral mechanic structure. (b) Schematic of analytic model of DLP system processing.

$$q_2 = \frac{2}{\sqrt{m}}\left(\frac{y}{a} + 0.5\right) \tag{14}$$

and

$$m = \frac{2\lambda(b-z)}{a^2} \tag{15}$$

where λ is the wavelength of light, and b represents the distance between the resin surface and the light mask. Hence, based on the Beer–Lambert Law, the equation that specifies the light energy absorbed by the resin is,

$$I(x,y,z) = I_d(x,y,z)\mathrm{e}^{-\varphi z} \tag{16}$$

where φ is the rate of absorption of wavelength λ by the resin. Thus, the energy to which every point is exposed is given by $E(x, y, z) = I(x, y, z)t$, where t is the period of exposure.

2.3. DFEM simulation

A cubic element with eight nodes is used to reflect realistically the characteristics of the RP layer. The developed simulation code is based on the dynamic finite element method. Fig. 3 shows a flowchart of the simulation process. The liquid mesh is pre-created and read into a matrix core, as shown in Fig. 4, which is an "H-4" diagnostic part [4,13,14]. This case study involves 1680 elements and 2366 nodes. Table 1 presents the parameters used in the simulation. The simulation of the DFEM yields the displacement of every node of the part. This information can be used to improve the profile of the part after deformation, and yield the new matrix of every node after compensation. Fig. 5(a) shows the simulated three-dimensional deformation of the "H-4" part. In this figure, the deformation of every node is very small. The

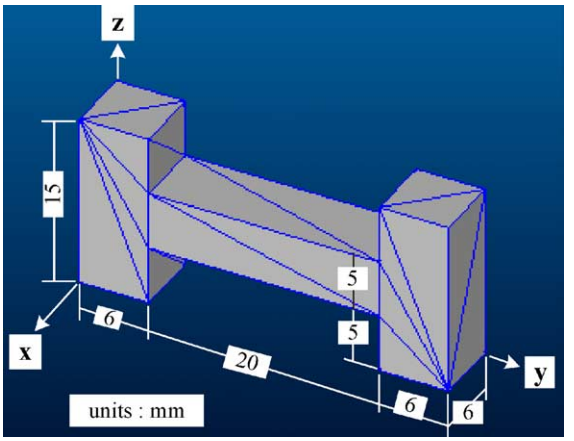

Fig. 9. Prototype of "H-4" solid (STL file).

Table 1
The parameters of experiment and simulation

Part	Element number	Node number	Thickness (mm)	Layer	Exposure time (s)	Simulation time (min)
H-4 part	1680	2366	0.1	150	10	150

Note: Simulated in PC with p42.5G CPU, 512M RAM.

deformation of every node is increased by a factor of 5 and shown as a two-dimensional profile, as shown in Fig. 5(b), to clarify the deformation of the outer profile. Fig. 6 presents the simulated reverse compensated CAD meshes of the ''H-4'' part in the simulation. Fig. 7 presents the results after the compensation of the CAD mesh of the ''H-4'' part in the simulation.

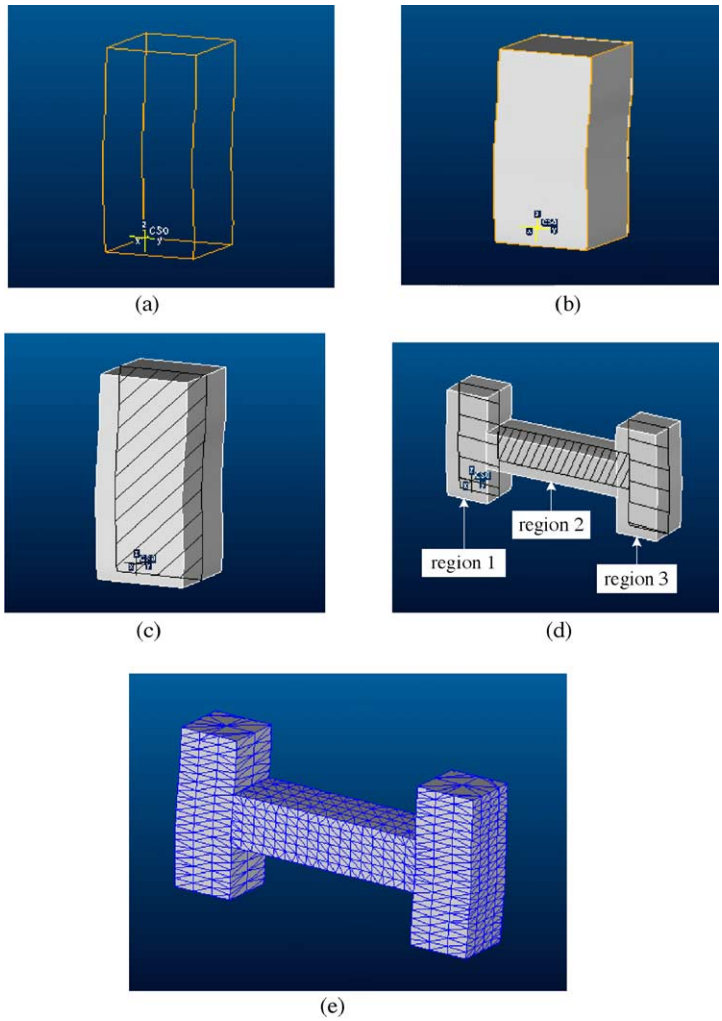

Fig. 10. The process of reverse compensation ''H-4'' model. (a) Curve diagram of region 1 profile by Pro/E .ibl file. (b) Create surface diagram of region 1 by curves. (c) Curve surfaces of region 1 merged to a solid model (cross section denotes solid model). (d) CAD model is assembled from all regions. (e) CAD file changed to a STL file.

3. Experimental apparatus

The photopolymer of the resin used in this study is NAF202, made by Nippon Kayaku Company. A special photo-initiator is added to NAF202 to initiate photo-polymerization in the range of visible light. The experimental apparatus is set up based on the principle of a mask-type stereolithographic rapid prototyping system, as shown in Fig. 8, at an expense of almost US$ 10,000. The system is one kind of bottom-exposure SL system and can be easily maintained and uses an inexpensive resin.

This experimental apparatus exposes the liquid resin at the bottom of the resin container to the platform, and an elevator driver controls the position of the platform. The distance between the platform and the bottom of the resin container is the thickness of the first layer that was fabricated. The platform rises when the current layer is completely solidified, and the liquid resin then fills the vacant region. The mask data of the next layer are simultaneously prepared. This procedure is repeated until the object is completely fabricated.

Most users use the term ''H-4'' [4,13,14] presented in Fig. 9 when evaluating the accuracy of three-dimensional SL products. Because the ''H-4'' part not only indicates bulk shrinkage but also indicate the bulk distortion. The ''H-4'' diagnostic part used in this study has the following process parameters: the

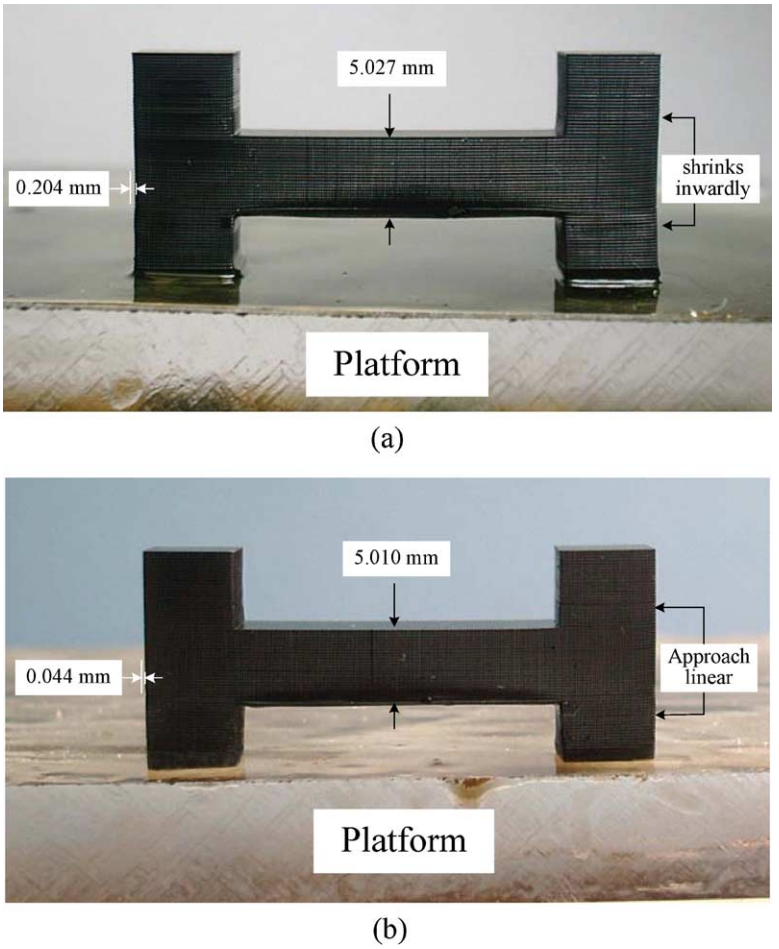

Fig. 11. ''H-4'' parts built by DLP mask-type RP system (for convenience of measurement, this figure is shown upside-down from the actual mechanic structure). (a) Deformation before compensation. (b) Deformation after compensation.

number of layers is 150; each slicing layer has a thickness of 0.1 mm, and the exposure time is 10 s per layer. These parameters are the same as those used in the simulation and presented in Table 1.

3.1. Design and production of reverse-compensation three dimension model

The original CAD and STL files of the required "H-4" part of the experiment were produced using the PRO/E software, as shown in Fig. 9. Two methods are used in designing the more complex reverse compensation three-dimensional CAD model. One is the use of reverse engineering software, and the other involves a series of procedures, firstly dividing the more complicated patterns into several simpler regions, and then completing each simpler region using PRO/E software. This software joins the points into curves; turns the curves into curved surfaces, and merges the curved surfaces into a solid model. Finally, the new reverse compensation CAD model is assembled from each finished simple region. This work applies the second method to reduce the use of package software.

In the design of the more complicated reverse compensation three-dimensional CAD model in this work, the "H-4" part is initially disconnected into three regions and then the new reverse compensation CAD model is assembled from each finished simple region. The procedure is as follows. First, the original coordinates and the distortion data of every node determined in the DFEM simulation are converted to an IBL file that can be accepted by PRO/E software, using the VB6.0 or C++ Builder program. Later, the IBL-formatted file is loaded into PRO/E software for processing. Consequently, the curved figure of the outer profile is produced, as required by the reverse compensation CAD model. Fig. 10(a) plots the relevant results. Secondly, the convergence curves of the profile are paved into a curved surface, as shown in Fig. 10(b). Thirdly, a solid model is produced through the formation and merging of the curved surfaces. The reverse compensation three-dimensional CAD model of a region is based on this model, as shown in Fig. 10(c). Fourthly, all of the completed regions are assembled into a actual reverse compensation CAD model, as shown in Fig. 10(d). The design of the reverse compensation three-dimensional CAD model is then completed by slicing the output in STL

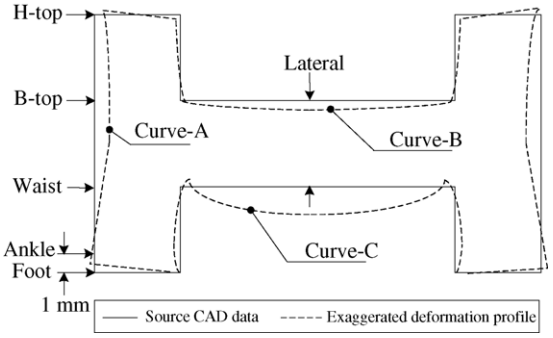

Fig. 12. Characteristic dimension and distortion trend of "H-4" part.

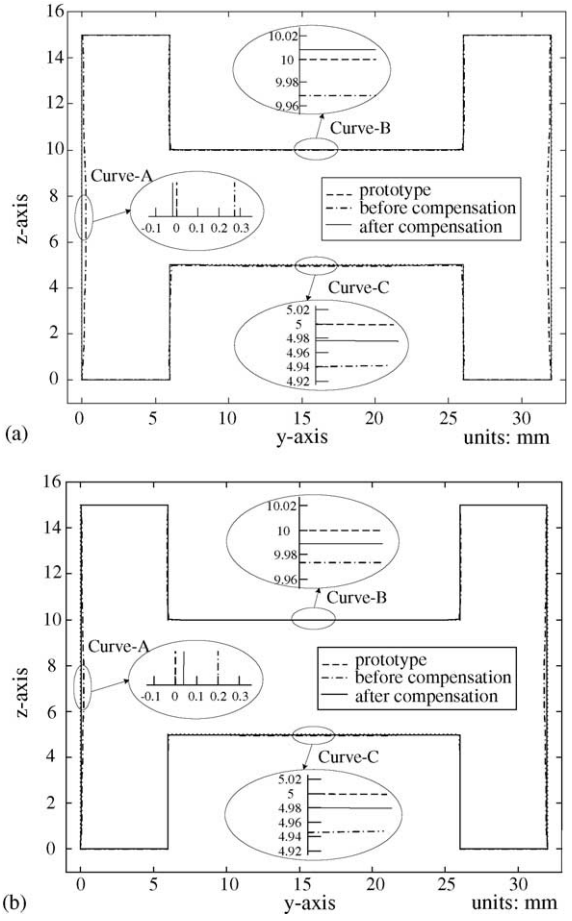

Fig. 13. Comparison of two-dimensional deformation of "H-4" part before and after compensation. (a) Deformation profile of simulation. (b) Deformation profile of experiment.

format, as shown in Fig. 10(e), and slicing the outputs in PRM and HPGL formats into layers using Autoedit2000 slicing software. Finally, it is loaded into the mask-type rapid prototyping system for practical fabrication. Fig. 11 presents the difference between the distortions before compensation with that after compensation, in cases of practical fabrication. This figure shows that all dimensions, apart from those of the lateral beam portion, were cured to within an error of 0.04 mm.

4. Results and discussion

In this section, "H-4" diagnostic parts before and after compensation are fabricated and simulated under the same conditions. A Coordinate Measuring Machine (CMM) from Mitutoyo-KN807 is used to measure the outer profiles of the part before and after compensation at every node. The experimentally obtained information can be used as reference data to support comparisons between simulated and experimental results. In this study, the deformed geometry of the "H-4" diagnostic part is such that six characteristic dimensions (H-top, B-top, waist, ankle, foot and lateral) are required to characterize the dimensional accuracy of SL products, as shown in Fig. 12. This finding was consistent with that of Cho and Park [14]. The solid line represents the CAD dimensions of the desired profile, and the dotted line represents a grossly exaggerated deformation profile for illustration. The three most distorted curves A–C are selected for further explanation, to elucidate the distortion of the curves before and after compensation determined by simulation and experiment, as shown in Fig. 12. Curve-A comprises the five characteristic dimensions of H-top, B-top, waist, ankle and foot. Curves B and C indicate the distortion in the characteristic lateral dimension. Fig. 13 presents the two-dimensional

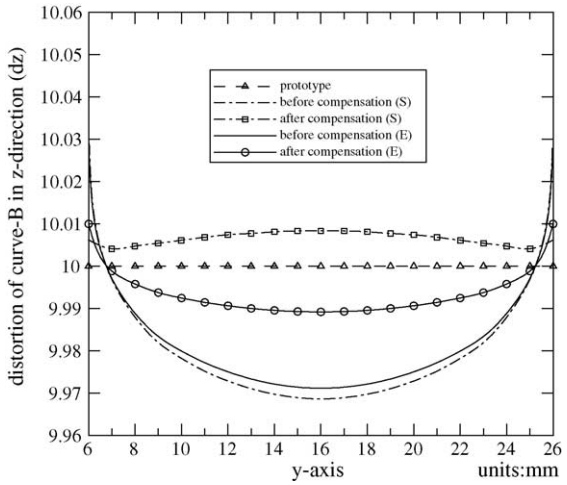

Fig. 15. Comparison of simulation and experimental results in curve-B of "H-4" part before and after compensation.

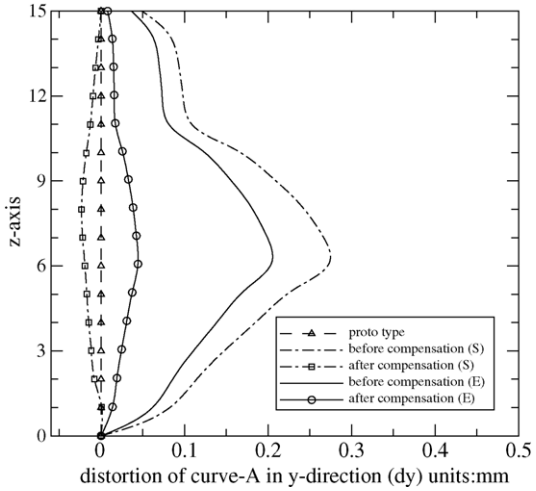

Fig. 14. Comparison of simulation and experimental results in curve-A of "H-4" part before and after compensation.

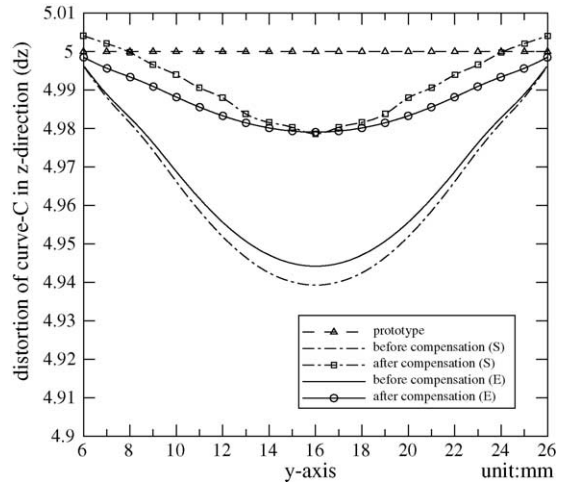

Fig. 16. Comparison of simulation and experimental results in curve-C of "H-4" part before and after compensation.

Table 2
Comparison of simulation and experimental distortions of curve-A of "H-4" part before and after compensation

Distortion of curve-A in *y*-direction (d*y*) (units: mm)				Improvement (%)
H-top	Simulation	Before	0.049	97.9
		After	0.001	
	Experiment	Before	0.037	78.4
		After	0.008	
B-top	Simulation	Before	0.159	89.3
		After	−0.017	
	Experiment	Before	0.119	78.2
		After	0.026	
The maximum distortion position	Simulation	Before	0.274	93.1
		After	−0.019	
	Experiment	Before	0.205	78.5
		After	0.044	
Waist	Simulation	Before	0.232	92.7
		After	−0.017	
	Experiment	Before	0.173	78.6
		After	0.037	
Ankle	Simulation	Before	0.085	98.8
		After	0.001	
	Experiment	Before	0.064	78.1
		After	0.014	

Note: (1) Negative values denote inverse deformation profile; (2) the maximum distortion position is nearly 1 mm above the waist position.

deformation before and after compensation of the "H-4" part. The three curves are greatly magnified to present the relationships among the distortions of curves A–C before and after compensation in a more detailed manner. Fig. 14 reveals the distortion of curve-A. This figure reveals that the distortions before and after compensation are similar, and the position of maximum distortion is almost 1 mm above the waist. The simulated maximum distortion of curve-A is reduced to −0.0194 mm from 0.2744 mm. Although it appears to be excessively compensated, the error is below 0.02 mm, and the maximum distortion of the experimental value in curve-A is reduced from 0.2049 to 0.0441 mm. Fig. 15 presents the distortion of curve-B. This figure shows that both the simulated and experimental results indicated that the error is reduced to under 0.011 mm. Fig. 16 plots distortion curve-C. Curve-C is associated with the first layer in the constructed lateral beam, so distortion curve-C affected not only by the buoyancy of the liquid resin but also by the bending stress caused by the weight of cured. Specifically, the downward distortion is greater before the first layer has been completely hardened than afterwards. These factors indicate that the error in curve-C after compensation exceeds those of curves A and B, but the compensation is nevertheless 60.3% in these cases. Tables 2 and 3 present the distortion values before and after compensation, corresponding to the three curves and the six characteristic dimensions. The data in Tables 2 and 3 prove that this research method is economic and effective.

Table 3
Comparison of simulation and experimental distortions of curve-B and curve-C of "H-4" part before and after compensation

Distortion of lateral beam in *z*-direction (d*z*) (units: mm)				Improvement (%)
Curve-B	Simulation	Before	0.032	75.0
		After	−0.008	
	Experiment	Before	0.029	62.1
		After	0.011	
Curve-C	Simulation	Before	0.061	65.6
		After	0.021	
	Experiment	Before	0.053	60.3
		After	0.021	

Note: Negative values denote inverse deformation profile.

5. Conclusion

Simulation by stereolithographic modeling and experiments on the ''H-4'' part are performed. This investigation applies a dynamic finite element method for simulating liquid stereolithography and compensating for the curl distortion caused by shrinkage. Subsequently, the simulated results are compared with the experimental results.

The results obtained herein support the following conclusions.

(1) This study focuses on developing and applying CAE simulation code to fabricate RP. A dynamic finite element method is successfully employed to simulate distortion, yielding highly accurate final parts by compensating for the original CAD model before the prototype is fabricated.
(2) Manufacturers can use the method proposed in this study to use lower-cost machines to increase the precision of the final parts, or obtain a more accurate precision on the same machines.
(3) Manufacturers can use the method in this study to avoid building a support for with a bending stress. However, the part is more accurately produced, reducing the time required for post-processing.
(4) The method herein can be applied whenever a finite element mesh can be established. Therefore, the method herein is not limited to simple parts, but can be applied to other parts with more complex geometries.
(5) This method is believed to be applicable to other materials or build-up methods used in RP fabrication. It yields more precise final parts, and can be extended to the application of RP in various industrial domains.
(6) The results can be further applied to micro-RP, to form a more accurate prototype.

Acknowledgements

The authors would like to thank the National Science Council of the Republic of China for financially supporting this research under Contract No. NSC92-2212-E011-001. The authors would also like to thank the rapid prototyping laboratory of the National Taiwan University of Science and Technology, Professor Alan C. Lin and Assistant Professor Y.L. Cheng for their useful suggestions.

Appendix A. Formula deduces

In this appendix, for the convenience to express, we substitute the strain rate $\{\dot{\varepsilon}\}$ for the increment of strain $\{\Delta\varepsilon\}$.

A.1. For elastic materials

From elastic Hooke's law

$$\{\dot{\varepsilon}^{\mathrm{e}}\} = [C^{\mathrm{e}}]\{\dot{\sigma}\}, \qquad \{\dot{\sigma}\} = \lfloor D^{\mathrm{e}} \rfloor \{\dot{\varepsilon}^{\mathrm{e}}\} \tag{A1}$$

and

$$[C^{\mathrm{e}}] = \frac{1}{E}\begin{bmatrix} 1 & -\mu & -\mu & 0 & 0 & 0 \\ -\mu & 1 & -\mu & 0 & 0 & 0 \\ -\mu & -\mu & 1 & 0 & 0 & 0 \\ 0 & 0 & 0 & 2(1+\mu) & 0 & 0 \\ 0 & 0 & 0 & 0 & 2(1+\mu) & 0 \\ 0 & 0 & 0 & 0 & 0 & 2(1+\mu) \end{bmatrix} \tag{A2}$$

$$[D^{\mathrm{e}}] = [C^{\mathrm{e}}]^{-1} = \frac{E}{1+\mu} \times \begin{bmatrix} \frac{1-\mu}{1-2\mu} & \frac{\mu}{1-2\mu} & \frac{\mu}{1-2\mu} & 0 & 0 & 0 \\ \frac{\mu}{1-2\mu} & \frac{1-\mu}{1-2\mu} & \frac{\mu}{1-2\mu} & 0 & 0 & 0 \\ \frac{\mu}{1-2\mu} & \frac{\mu}{1-2\mu} & \frac{1-\mu}{1-2\mu} & 0 & 0 & 0 \\ 0 & 0 & 0 & \frac{1}{2} & 0 & 0 \\ 0 & 0 & 0 & 0 & \frac{1}{2} & 0 \\ 0 & 0 & 0 & 0 & 0 & \frac{1}{2} \end{bmatrix} \tag{A3}$$

for example

$$\dot{\varepsilon}_x^{\mathrm{e}} = \frac{1}{E}[\dot{\sigma}_x - \mu(\dot{\sigma}_y + \dot{\sigma}_z)]$$

$$\dot{\varepsilon}_y^{\mathrm{e}} = \frac{1}{E}[\dot{\sigma}_y - \mu(\dot{\sigma}_z + \dot{\sigma}_x)]$$

$$\dot{\varepsilon}_z^{\mathrm{e}} = \frac{1}{E}[\dot{\sigma}_z - \mu(\dot{\sigma}_x + \dot{\sigma}_y)] \tag{A4}$$

and

$$\dot{\varepsilon}_k = \dot{\varepsilon}_x^{\mathrm{e}} + \dot{\varepsilon}_y^{\mathrm{e}} + \dot{\varepsilon}_z^{\mathrm{e}} = \frac{1-2\mu}{E}(\dot{\sigma}_x + \dot{\sigma}_y + \dot{\sigma}_z) \tag{A5}$$

$$G = \frac{E}{2(1+\mu)}, \qquad k = \frac{E}{3(1-2\mu)} \tag{A6}$$

where $\{\dot{\varepsilon}^{\mathrm{e}}\}$ represents the elastic strain rate; $\{\dot{\sigma}\}$ is the stress rate; $\lfloor C^{\mathrm{e}} \rfloor$ is the elastic flexibility matrix; $\lfloor D^{\mathrm{e}} \rfloor$ is the elastic stress–strain matrix; $\{\dot{\varepsilon}_k\}$ is the volume strain rate; E is the elastic modulus; μ is the Poisson's ratio; G is the shear modulus; k is the volume modulus;

A.2. For viscous–elastic–plastic materials

Constitutive equations of Maxwell model for viscous–elastic–plastic materials is expressed by [11]:

$$\{\dot{\varepsilon}\} = \{\dot{\varepsilon}^{\mathrm{e}}\} + \{\dot{\varepsilon}^{\mathrm{T}}\} + \{\dot{\varepsilon}^{\mathrm{v}}\} + \{\dot{\varepsilon}^{\gamma}\} + \{\dot{\varepsilon}^{\mathrm{p}}\} \tag{A7}$$

During photo-polymerization, the plastic strain rate $\{\dot{\varepsilon}^{\mathrm{p}}\}$ is low and can be neglected. Thus, Eq. (A7) can be rewritten as:

$$\{\dot{\varepsilon}\} = \{\dot{\varepsilon}^{\mathrm{e}}\} + \{\dot{\varepsilon}^{\mathrm{T}}\} + \{\dot{\varepsilon}^{\mathrm{v}}\} + \{\dot{\varepsilon}^{\gamma}\} \tag{A8}$$

and

$$\{\dot{\varepsilon}^{\mathrm{v}}\} = \{\dot{\varepsilon}^{d}\} + \{\dot{\varepsilon}^{k}\} = \frac{1}{2\eta_G}\{\sigma'\} + \frac{1}{3\eta_k}\{\sigma_{\mathrm{m}}\} \tag{A9}$$

$$t_G = \frac{\eta_G}{G}, \qquad t_k = \frac{\eta_k}{k} \tag{A10}$$

$$\begin{aligned} \sigma'_x &= \tfrac{1}{3}(2\sigma_x - \sigma_y - \sigma_z), \\ \sigma'_y &= \tfrac{1}{3}(2\sigma_y - \sigma_z - \sigma_x) \\ \sigma'_z &= \tfrac{1}{3}(2\sigma_z - \sigma_x - \sigma_y), \end{aligned} \tag{A11}$$

$$\sigma_{\mathrm{m}} = \tfrac{1}{3}(\sigma_x + \sigma_y + \sigma_z) \tag{A12}$$

where $\{\dot{\varepsilon}\}$ is the Euler strain rate; $\{\dot{\varepsilon}^{\mathrm{e}}\}$ represents the elastic strain rate; $\{\dot{\varepsilon}^{\mathrm{T}}\}$ is the thermal strain rate that can be rewritten as $\{\alpha\dot{T}\}$; $\{\dot{\varepsilon}^{\mathrm{v}}\}$ is the viscous strain rate that is the function of time, so it can be expressed as $\{\sigma(t)\}$ [11]; $\sigma(t)$ represents the nodal viscous stress that is the function of time (t); $\{\dot{\varepsilon}^{\gamma}\}$ is the strain rate caused by cure shrinkage and is given by $\Delta\beta(I, t)$, which is a function of the intensity of that light (I) and elapsed time (t); $\{\dot{\varepsilon}^{d}\}$ and $\{\dot{\varepsilon}^{k}\}$ are two components of viscous strain rate $\{\dot{\varepsilon}^{\mathrm{v}}\}$ in the shear component and volume component relatively; η_G and η_k are the viscous coefficient in the shear deformation and volume deformation relatively; G is the shear modulus; k is the volume modulus; t_G and t_k are the slack time relatively G and k; $\{\sigma'\}$ is the deviatoric stress; $\{\sigma_{\mathrm{m}}\}$ is the mean stress. By substituting Eq. (A9) into (A8), yields the following equation:

$$\begin{Bmatrix} \dot{\varepsilon}_x \\ \dot{\varepsilon}_y \\ \dot{\varepsilon}_z \\ \dot{\gamma}_{yz} \\ \dot{\gamma}_{zx} \\ \dot{\gamma}_{xy} \end{Bmatrix} = \begin{Bmatrix} \dot{\varepsilon}_x^{\mathrm{e}} \\ \dot{\varepsilon}_y^{\mathrm{e}} \\ \dot{\varepsilon}_z^{\mathrm{e}} \\ \dot{\gamma}_{yz}^{\mathrm{e}} \\ \dot{\gamma}_{zx}^{\mathrm{e}} \\ \dot{\gamma}_{xy}^{\mathrm{e}} \end{Bmatrix} + \begin{Bmatrix} \alpha\dot{T} \\ \alpha\dot{T} \\ \alpha\dot{T} \\ 0 \\ 0 \\ 0 \end{Bmatrix} + \frac{1}{2\eta_G} \begin{Bmatrix} \sigma'_x \\ \sigma'_y \\ \sigma'_z \\ 2\tau_{yz} \\ 2\tau_{zx} \\ 2\tau_{xy} \end{Bmatrix} + \frac{1}{3\eta_k} \begin{Bmatrix} \sigma_{\mathrm{m}} \\ \sigma_{\mathrm{m}} \\ \sigma_{\mathrm{m}} \\ 0 \\ 0 \\ 0 \end{Bmatrix} + \begin{Bmatrix} \Delta\beta(I) \\ \Delta\beta(I) \\ \Delta\beta(I) \\ 0 \\ 0 \\ 0 \end{Bmatrix} \tag{A13}$$

Substituting Eqs. (A11), (A12) into (A13), yields the following equation:

$$\begin{Bmatrix} \dot{\varepsilon}_x^{\mathrm{e}} \\ \dot{\varepsilon}_y^{\mathrm{e}} \\ \dot{\varepsilon}_z^{\mathrm{e}} \\ \dot{\gamma}_{yz}^{\mathrm{e}} \\ \dot{\gamma}_{zx}^{\mathrm{e}} \\ \dot{\gamma}_{xy}^{\mathrm{e}} \end{Bmatrix} = \begin{Bmatrix} \dot{\varepsilon}_x \\ \dot{\varepsilon}_y \\ \dot{\varepsilon}_z \\ \dot{\gamma}_{yz} \\ \dot{\gamma}_{zx} \\ \dot{\gamma}_{xy} \end{Bmatrix} - \begin{Bmatrix} \alpha\dot{T} \\ \alpha\dot{T} \\ \alpha\dot{T} \\ 0 \\ 0 \\ 0 \end{Bmatrix} - [D^{\eta k}] \times \begin{Bmatrix} \sigma_x \\ \sigma_y \\ \sigma_z \\ \tau_{yz} \\ \tau_{zx} \\ \tau_{xy} \end{Bmatrix} - \begin{Bmatrix} \Delta\beta(I) \\ \Delta\beta(I) \\ \Delta\beta(I) \\ 0 \\ 0 \\ 0 \end{Bmatrix} \tag{A14}$$

where

$$[D^{\eta k}] = \frac{1}{18\eta_G\eta_k}\begin{bmatrix} 2\eta_G+6\eta_k & & & & & & \\ 2\eta_G-3\eta_k & 2\eta_G+6\eta_k & & & \text{symmetric} & & \\ 2\eta_G-3\eta_k & 2\eta_G-6\eta_k & 2\eta_G+6\eta_k & & & & \\ 0 & 0 & 0 & 18\eta_k & & & \\ 0 & 0 & 0 & 0 & 18\eta_k & & \\ 0 & 0 & 0 & 0 & 0 & 18\eta_k & \\ 0 & 0 & 0 & 0 & 0 & 0 & 18\eta_k \end{bmatrix}$$

Substituting Eqs. (A10), (A14) into (A1), yields the following equation:

$$\begin{Bmatrix} \dot\sigma_x \\ \dot\sigma_y \\ \dot\sigma_z \\ \dot\tau_{yz} \\ \dot\tau_{zx} \\ \dot\tau_{xy} \end{Bmatrix} = [D^{\mathrm{e}}]\begin{Bmatrix} \dot\varepsilon_x \\ \dot\varepsilon_y \\ \dot\varepsilon_z \\ \dot\gamma_{yz} \\ \dot\gamma_{zx} \\ \dot\gamma_{xy} \end{Bmatrix} - \frac{E}{1-2\mu}\begin{Bmatrix} \alpha\dot T \\ \alpha\dot T \\ \alpha\dot T \\ 0 \\ 0 \\ 0 \end{Bmatrix} - [t^{\eta k}]\begin{Bmatrix} \sigma_x \\ \sigma_y \\ \sigma_z \\ \tau_{yz} \\ \tau_{zx} \\ \tau_{xy} \end{Bmatrix} - \frac{E}{1-2\mu}\begin{Bmatrix} \Delta\beta(I) \\ \Delta\beta(I) \\ \Delta\beta(I) \\ 0 \\ 0 \\ 0 \end{Bmatrix} \tag{A15}$$

and

$$[t^{\eta k}] = \begin{bmatrix} t_G+2t_k & & & & & \\ t_G-t_k & t_G+2t_k & & \text{symmetric} & & \\ t_G-t_k & t_G-t_k & t_G+2t_k & & & \\ 0 & 0 & 0 & 3t_k & & \\ 0 & 0 & 0 & 0 & 3t_k & \\ 0 & 0 & 0 & 0 & 0 & 3t_k \end{bmatrix} \tag{A16}$$

where $[t^{\eta k}]$ is the slack time matrix that is the function of time (t), so $\{\dot\varepsilon^{\mathrm{v}}\}$ it can be expressed as $\{\sigma(t)\}$ [11], where $\{\sigma\}$ represents the nodal viscous stress that is the function of time (t).

Substituting Eq. (A6) into (A15), thus Eq. (A15) can be rewritten as:

$$\{\dot\sigma\} = [D^{\mathrm{e}}]\{\dot\varepsilon\} - 3k\{\alpha\dot T\} - \{\sigma(t)\} - 3k\{\Delta\beta(I)\} \tag{A17}$$

Matching the relation of finite elements:

$$\{\dot\varepsilon\} = [B]\{\dot u\} \tag{A18}$$

Substituting Eq. (A18) into (A17) and $\int_v [B]^{\mathrm{T}}\,\mathrm{d}V$ into the virtual work principle, yields the following equation for viscous–elastic–plastic materials is expressed

$$\int_v [\delta\dot e]\{\dot\sigma\}\,\mathrm{d}V = \int_v [[B]^{\mathrm{T}}[D^{\mathrm{e}}][B]\{\dot u\} - [B]^{\mathrm{T}}\{\sigma\} - [B]^{\mathrm{T}}(3k)\{\alpha\dot T + \Delta\beta(I)\}]\,\mathrm{d}V = 0 \tag{A19}$$

Consequently, the constitutive equation in the dynamic finite element analysis of the stereolithographic process can be expressed as:

$$[K]\{\dot u\} - \{\dot f\} = 0 \tag{A20}$$

where

$$[K] = \int_v [B]^{\mathrm{T}}[D^{\mathrm{e}}][B]\,\mathrm{d}V \tag{A21}$$

$$\{\dot f\} = \int_v [[B]^{\mathrm{T}}\{\sigma\} + [B]^{\mathrm{T}}(3k)\{\alpha\dot T + \Delta\beta(I)\}]\,\mathrm{d}V \tag{A22}$$

In the above equation, $[K]$ is the stiffness matrix; $\{\dot{u}\}$ is the increment in nodal displacement; $\{\dot{f}\}$ is increment in the effective nodal force; $[\delta\dot{e}]$ is the velocity gradient; $[B]$ represents the strain rate–velocity matrix; $[B]^{\mathrm{T}}$ is the transpose of the matrix $[B]$; $\{\sigma\}$ represents the nodal viscous stress that is the function of time (t).

References

[1] P.F. Jacobs, Rapid Prototyping and Manufacturing Fundamentals of Stereolithography, ASME Press, New York, 1992.

[2] H. Narahara, et al. Reaction heat effects on initial linear shrinkage and deformation in stereolithography, Rapid Prototyping Journal 5 (3) (1999) 120–128.

[3] G. Bugeda, et al. Numerical analysis of stereolithography processes using the finite element method, Rapid Prototyping Journal 1 (2) (1995) 12–23.

[4] F. Tanaka, et al. Thermal distortion analysis during photopolymerization in stereolithography, in: Proceedings of the 8th International Conference on Rapid Prototyping, Tokyo, Japan, 2000, pp. 87–92.

[5] Y.M. Huang, et al. Computer supported force analysis and layer imagine for masked rapid prototyping system, in: Proceedings of the 6th International Conference on Computer Supported Cooperative Work in Design, Ontario, Canada, 2001, pp. 562–567.

[6] T. Murakami, et al. Refrigerative stereolithography using direct masking, in: Proceedings of the 8th International Conference on Rapid Prototyping, Tokyo, Japan, 2000, pp. 184–189.

[7] T. Hatashi, et al. Direct 3D forming using TFT LCD mask, in: Proceedings of the 8th International Conference on Rapid Prototyping, Tokyo, Japan, 2000, pp. 172–177.

[8] Y.M. Huang, C.P. Jiang, Curl distortion analysis during photopolymerization of stereolithography using dynamic finite element method, International Journal of Advance Manufacturing Technology 21 (2003) 586–595.

[9] Y.M. Huang, C.P. Jiang, Numerical analysis of mask type stereolithography process using dynamic finite element method, International Journal of Advance Manufacturing Technology 21 (2003) 649–655.

[10] T. Hatakeyama, F.X. Quinn, Thermal Analysis and Application to Polymer Science, John Willey & Sons, 1994.

[11] Y. Yoshiaki, Yamada, Viscous–elasticity–plasticity, Baifu-Kan, 1980(Japanese).

[12] V.K. Varadan, X. Jiang, V.V. Varadan, Microstereolithography and other Fabrication Techniques for 3D MEMS, John Wiley & Sons, 2001.

[13] Y.M. Huang, J.Y. Jeng, C.P. Jiang, J.C. Wang, Increased accuracy by using dynamic finite element method in the constrain–surface stereolithography system, Journal of Material Processing Technology 140 (2003) 191–196.

[14] H.S. Cho, W.S. Park, Determining optimal parameters for stereolithography processes via genetic algorithm, Journal of Manufacturing Systems 19 (1) (2000) 18–34.

You-Min Huang received the BS degree in mechanical engineering from Tamkung University, Taipei, Taiwan, ROC, in 1974, and the Doctor of Engineering degree in mechanical engineering from the University of Tokyo, Tokyo, Japan in 1981. He currently is a professor of the Department of Mechanical Engineering, National Taiwan University of Science and Technology, Taipei, Taiwan. His primary research focuses in the area of sheet metal forming processes analysis, rapid prototyping processes analysis, etc. He is a member of CSME, and serves as an associate editor for the *Journal of the Chinese Society of Mechanical Engineering*. He is also a Secretary General of SME Taipei Chapter.

Hsiang-Yao Lan is a lecturer in the Department of Mechanical Engineering, China Institute of Technology. He received his BS degree in 1987 and the MS degree in 1990, from the Department of Mechanical Engineering, National Taiwan University of Science and Technology. He is currently a graduate student of PhD degree course. His research interests in the numerical analysis of 3D CAD/CAE/CAM and rapid prototyping.